# Effect of the Submerged Vortex Cavitation Occurred in Pump Suction Intake on Hydraulic Forces of Mixed Flow Pump Impeller

Takahide NAGAHARA, Tadashi SATO and Tomoyoshi OKAMURA
Tsuchiura Products Division, Industrial Machinery Systems Division, Hitachi, Ltd.,
603 Kandatsu-machi, Tsuchiura-shi, Ibaraki 300-0013, Japan

## Abstract

The effect of submerged vortices on the hydraulic forces of a mixed flow pump impeller was studied using a model pump with an intake sump. The experiments comprise observation of submerged vortices reaching the impeller with a high-speed video camera and measurement of the velocity distribution around the submerged vortex by PTV (particle tracking velocimetry) to obtain the strength of the vortex. Measurement results are compared with CFD (computational fluid dynamics) calculation to evaluate their accuracy. Hydraulic forces on the model pump when the submerged vortex reached the pump impeller was measured with load cells. The relationship between the strength of the submerged vortex and the effect of the vortex on the fluctuation of the hydraulic forces are described.

## 1 Introduction

Smaller pump stations for power plants and drainage pump stations are seen as a means of reducing construction costs. The consequent trend implies that the mean flow velocity at the pump suction intake sump has been increasing, which in turn increases the potential for submerged vortex cavitation and air entraining vortex. These kinds of strong vortex cause vibration and noise in pumps.

Especially in the case of submerged vortex cavitation, interest has focused on the inception of cavitation in the vortex region and observation of various types of vortices. Arndt and Keller (1992) investigated water quality effects on the inception of tip vortex cavitation. Rajendran, Constantinescu and Patel (1998) compared numerical simulation results with experimental measurements to investigate the flow condition in the model pump intake sump and to evaluate the accuracy of the numerical simulation results. Recently Shibata et al. (2000) described a new method of predicting submerged vortices that uses CFD with a vortex model. These studies were carried out to design an optimum pump intake configuration without these vortices. There are some papers concerning the blade-vortex interaction; for example, Krishnamoorthy and Marshall (1998) have investigated three-dimensional blade-vortex interaction using flow visualization experiments and computer simulations. However, these investigations were carried out under the single-phase flow condition. Concerning submerged vortex cavitation in particular, there have been no quantitative data.

Submerged vortex cavitation when it interacts with the pump impeller affects the pump's reliability. Thus it is necessary to investigate its effects to establish reliable guidelines for the design of trouble-free pumps and intakes. Knowledge of these effects will lead to the development of next-generation pumps with increased intake velocity and weak vortex occurrence will be permissible in that pump operation.

In this study, to obtain quantitative data of the effect of the submerged vortex's strength on the hydraulic forces of the pump impeller, we created a special experimental equipment that has a model intake sump including a model pump with an impeller and built-in load cells. The experiments comprised observation of submerged vortices reaching the impeller with a high-speed video camera and measurement of the velocity distribution around the submerged vortex by PTV (particle tracking velocimetry) to obtain the strength of the vortex. The diameter of the submerged vortex cavitation was measured using a digital image processing system. Numerical simulation of the flow was also done to evaluate the measurement data.

## 2 Experimental equipment and numerical calculation

Figures 1 and 2 show a schematic diagram of the experimental equipment and the observation area of the submerged vortex occurring in the lower part of the pump bell. The experimental equipment has a pressure tank that can control the pump inlet pressure, also cavitation number. The intake's rectangular channel is divided into two sections by the center pier in the upper stream region of the pump suction sump and two valves connect each approach pipes.

The distribution of flow rate of each channel is controlled by two valves and measured by two electromagnetic flow meters in the return circuit. Therefore, the magnitude of pump inlet swirl flow which cause the submerged vortex cavitation is changed by controlling the pump capacity and the distribution of flow rate for the two channels. The experiment was done using the following configuration parameter: height from the bottom to the bell normalized with respect to the bell diameter, $H_b/D_b$=0.5 and 0.93. The Reynolds number, based on the pump bell diameter $D_b$ and the mean velocity at the bell, was on the order of $10^5$.

The tangential velocities around the submerged vortex were measured by PTV and a high-speed video recorder as shown in Figure 2. Small bubbles and nuclei in water were used as the tracer. The diameter of the submerged vortex cavitation area (visible part of the submerged vortex) was measured by a digital image processing system using the image data of the vortex.

A mixed flow pump was used as the test model pump as shown in Figure 2. Its specifications are listed in Table 1. The load cells included in the model pump measured the fluctuation of the radial and axial forces whenever a submerged vortex occurred and reached the model pump impeller.

The numerical calculations were carried out on a grid of approximately 1,000,000 points that included the intake sump and the model pump with impeller. The calculation was applied a numerical calculation code that solve the time-averaged Navier-Stokes equations with the RNG k-ε turbulence model using a cell-centered finite volume method.

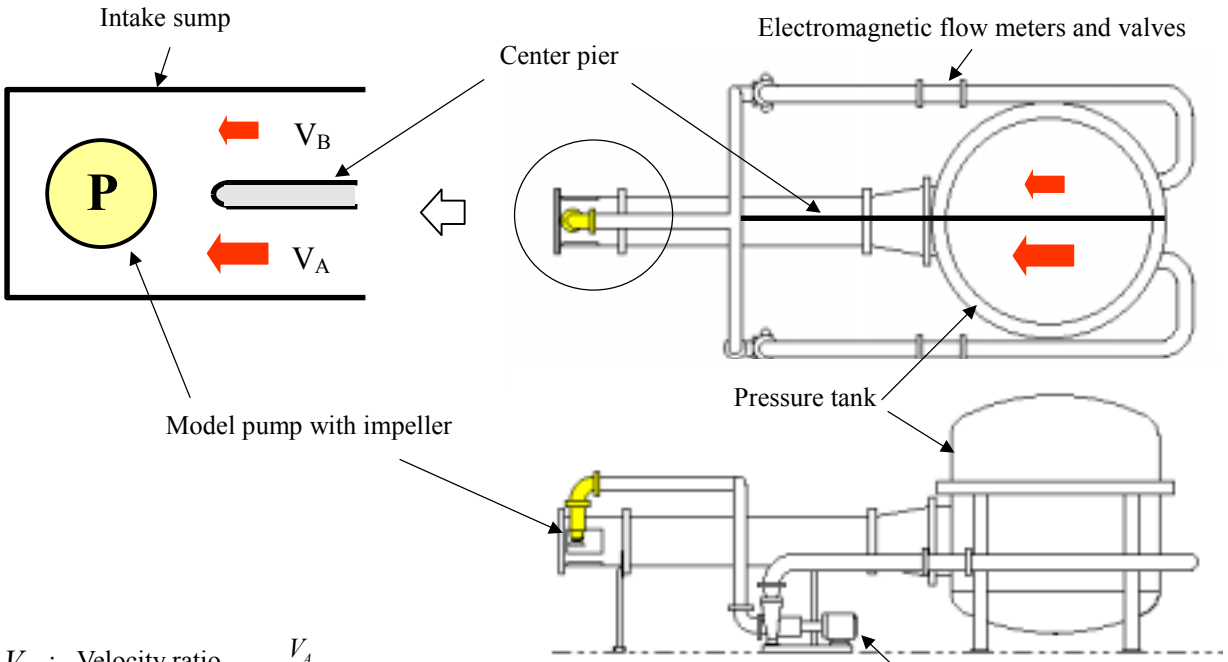


Figure 1. Schematic diagram of the experimental equipment.

Table 1. Specification of the model pump.

| | |
|---|---|
| Specific speed | Ns: 1300 (rpm,$m^3$/min,m) |
| Pump speed | N: 2000 ($min^{-1}$) |
| Impeller diameter | $D_2$: 100 (mm) |

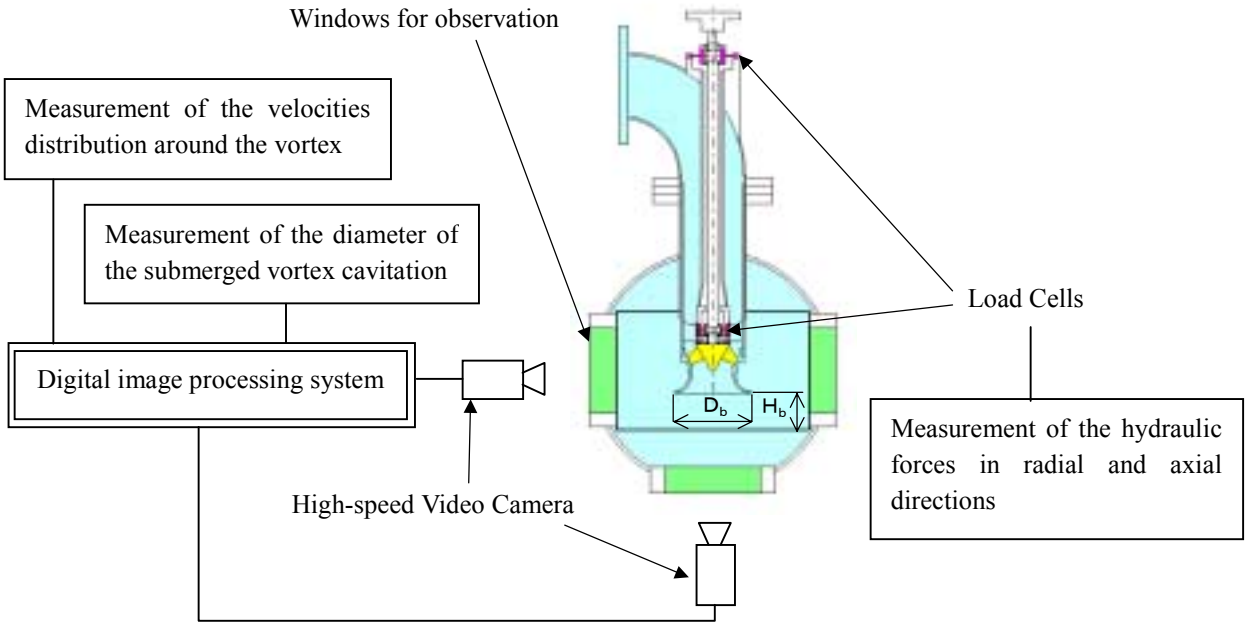


$D_b$ : Bell mouth diameter

$H_b$ : Clearance between bell mouth and bottom

Figure 2. Schematic diagram of the measurement system.

## 3 Inception of submerged vortex cavitation

A submerged vortex cavitation generally occurs when the mean velocity of intake sump increases. The critical velocities of cavitation inception mainly depend on the mean velocity, velocity distribution of upper flow and pressure. Figure 3 shows the relationship between the critical velocity of inception and $V_R$. $V_R$ denotes the ratio of the mean velocities of each channel that divided by the center pier at the upper stream region of the intake sump, i.e., $V_R=V_A/(V_A+V_B)$. This parameter represents the degree of approach skewed flow distribution. The critical mean approach velocity ($V=(V_A+V_B)/2$) that divided by the velocity at the best efficiency point of the capacity in the model pump performance curve is denoted as $V_{cr}/ V_{100\%Q}$. The critical velocity was measured as the velocity that the visible submerged vortex cavitation disappeared (the velocity at the desinent cavitation number). The pump inlet pressure at the experimental condition was 0.1 MPa.

The critical velocities roughly decrease in proportion as the ratio of the mean velocity increase. Increasing of the strength of swirl flow given by the velocity distribution of upstream mainly cause this result. Figure 4 shows the typical submerged vortex cavitation appearance in the model pump and the intake sump. The vortex cavitation occurred from a floor of the sump to the pump inlet and reached the impeller.

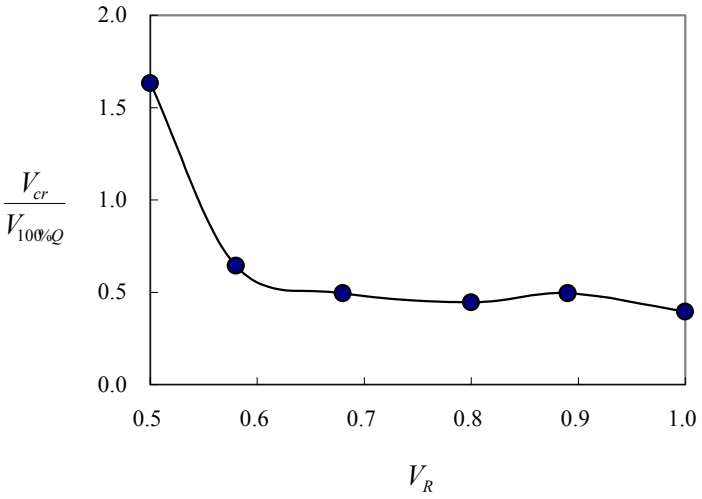


Figure 3. The relationship between critical velocity of cavitation inception and the ratio of the mean velocity.

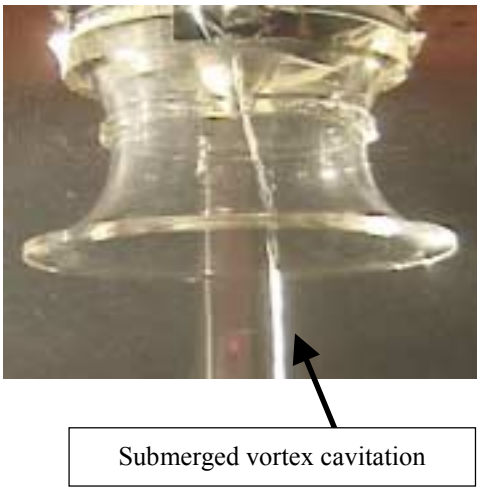


Figure 4. Observed submerged vortex cavitation in the intake sump.

## 4 Velocity distribution around the submerged vortex

Figure 5 shows the measurement results of the tangential velocity distribution around the submerged vortex for the configuration parameter of $H_b/D_b$=0.5. $V_R$ is the parameter that denotes the degree of approach skewed flow distribution as mentioned above. The measurements were carried out at the capacity of the best efficiency point in the performance curve of the model pump and at 120% of that capacity. The mean approach velocity at the best efficiency point and at 120% of that capacity are denoted as $V_{100\%Q}$ and $V_{120\%Q}$ respectively. The horizontal axis $r/D_b$ indicates the distance from the center of the vortex normalized by the pump bell diameter, and the vertical axis is the tangential velocities of the normalized by mean approach velocities.

As shown in Figure 5, the tangential velocity distribution around the submerged vortex is that of a free vortex. The tangential velocities tend to increase in proportion as the capacity Q and the ratio of the mean velocity, $V_R$ increase.

The relationship of the circulation, $\Gamma/D_bV_{100\%Q}$, and $V_R$ is shown in Figure 6. The circulation is normalized with respect to the pump bell diameter and mean approach velocity. The circulation was also obtained from the velocity distribution result in Figure 5 and calculated using the following formula, using the tangential velocities, $V_\theta$, and the distance from the center of the submerged vortex, r.

$$\Gamma = 2\pi r V_\theta$$

In Figure 6, the calculated values of the circulation around the submerged vortex are plotted to evaluate the experimental data. The calculated values were obtained by special method that calculate the circulation around analytically identified vortex portions using the global velocity distribution calculated by above mentioned simulation code. (Shibata et al. 2000) The calculated flow pattern for the lower part of the pump bell is shown in Figure 7.

As shown in Figure 6, the circulation of the submerged vortex increases in proportion $V_R$. This result indicates that the circulation of the submerged vortex is mainly caused by the upper stream velocity distortion; therefore, the strength of the submerged vortex can be controlled systematically using, $V_R$.

The measured values of circulation qualitatively agree with calculated ones. However, quantitatively, they differ up to about 30%. The values calculated by numerical simulation are generally lower than the experimental ones. In this investigation, the measurement technique was very simple (no laser equipment was used), and small air bubbles (similar to nuclei) in the water were used for the tracer to measure velocities (using PTV). The numerical calculation was carried out as a single-phase flow. Therefore, both calculation and measurement have the possibility of error and we will have to investigate the cause of this discrepancy in detail in the next research. Note that although the measurement technique is very simple, the measured values were obtained properly.

.

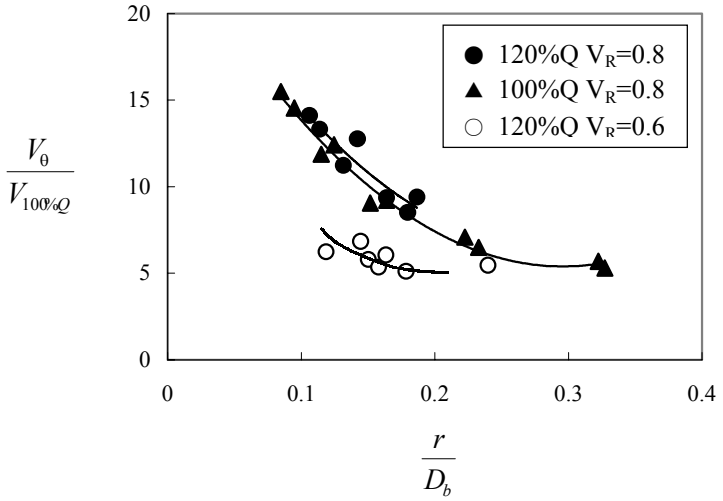


Figure 5. Measurement result of the tangential velocity distribution around the submerged vortex.

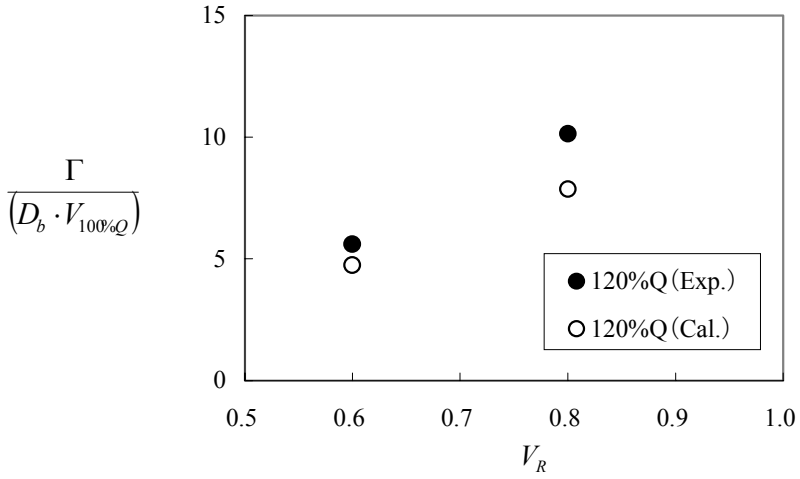


Figure 6. The relationship between velocity ratio and circulation of submerged vortex including comparison of calculation result by CFD.

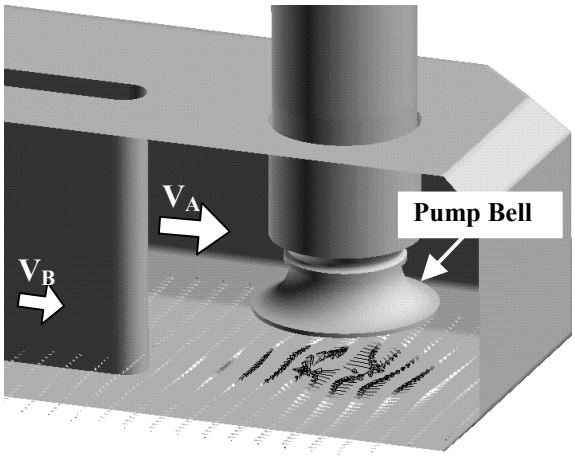


Figure 7. Calculated result for the lower section of the pump.

Figure 8 shows the relationship between the circulation's normalized intake mean velocity and pump bell diameter, $\Gamma/D_bV_{100\%Q}$, and the diameter of the cavitation area of the submerged vortex normalized by the bell diameter, $d_c/D_b$. The diameter of the cavitation area was measured using a digital image processing system, based on the image data of the visible submerged vortex taken by the high-speed video recorder. The diameter of the cavitation area correlated with circulation of submerged vortex. The diameters increase in proportion to the circulation increase of the submerged vortex. This result indicates the region in which the pressure became less than the vapor pressure expanded radially from the center of the vortex because of the increase in the tangential velocities of the vortex.

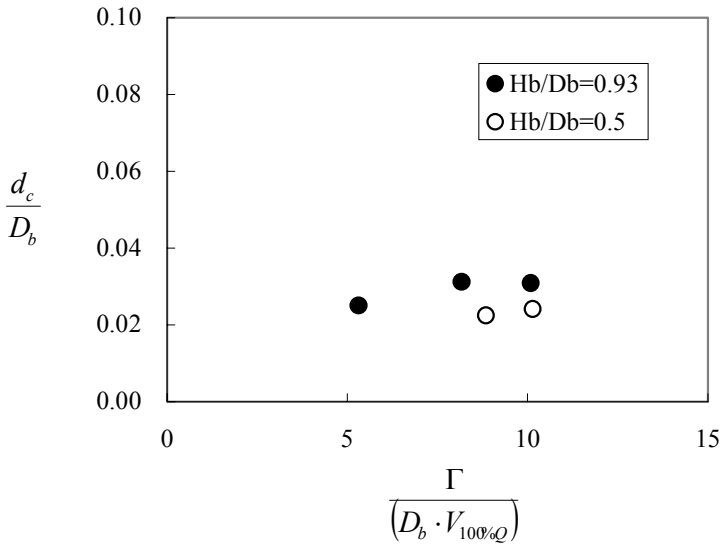


Figure 8. The relationship between circulation of the submerged vortex and the diameter of the cavitation area.

# 5 The effects of a submerged vortex interacting with pump impeller

Using the relationship between the strength of the submerged vortex and the size of the cavitation area, we examined the effect of the submerged vortex strength interacting with the model pump impeller on hydraulic forces in the radial and axial directions.

Figure 9 shows the relationship between the diameter of the cavitation area at the submerged vortex normalized by pump bell diameter, $d_c/D_b$, and the rate of increase in fluctuation of the hydraulic forces in the radial and axial directions. $F_c/F_{nc}$ in the figure is the root mean square of the hydraulic forces measured when the submerged vortex reached model pump impeller, $F_c$, divided by the forces measured without the submerged vortex in the high system pressure, $F_{nc}$. The fluctuation value generally increases in proportion to the diameter of the cavitation area of the submerged vortex. The maximum diameter $d_c/D_b$ was 0.032, and for this value, the maximum rate of increase in hydraulic force reached approximately 1.4 times that measured without submerged vortex cavitation.

The submerged vortex interacting with the model pump impeller observed using the high-speed video recorder as shown in Figure 10. Both pictures (each taken at the different times) were for the same capacity and ratio of mean velocity. The submerged vortex was always present, but its shape continually changed. In the left photo it goes from the side of the impeller cap to the impeller blades, and in the right photo it splits into thin spiral vortices before reaching the impeller. In this study, differences in vortex shape were not considered in the measurement of the hydraulic forces. The dispersion of the measurement data in Figure 9 may have been in part due to differences in vortex shape.

This observation result suggests the possibility that thin vortices in rotating flow formed one strong submerged vortex.

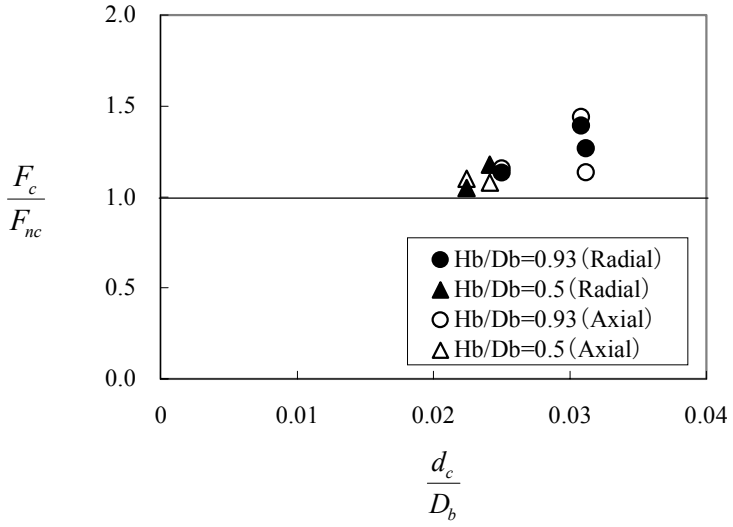


Figure 9. The relationship between diameter of cavitation area and the rate of increase in fluctuation of the hydraulic forces compared to measurement values without vortex.

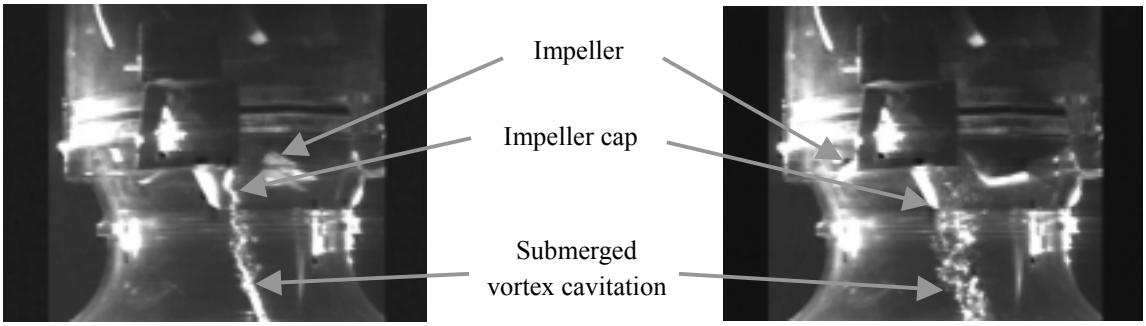


Figure 10. Observed submerged vortex cavitation at different moments.
(flow direction is the normal to the paper)

# 6 Conclusions

We studied the effect of submerged vortices on hydraulic forces of a mixed flow pump impeller by using a model pump with an intake sump. To obtain the strength of the submerged vortex, the tangential velocities and the diameter of the cavitation area were measured by means of a high-speed video recorder and a digital image processing system. The effect of a submerged vortex whose strength was already known on the hydraulic forces of the model pump was investigated. The following conclusions were obtained.

(1) It is confirmed that the strength of submerged vortices was in the control of the upper stream velocity distortion given systematically. The circulation increased in proportion to the velocity ratio of the upstream channels.

(2) The diameter of the cavitation area of the submerged vortex correlated with the circulation of the vortex. The diameter increased in proportion to the circulation of the submerged vortex.

(3) The measured values of circulation qualitatively agreed with the calculated values.

(4) The diameter of the cavitation area of the submerged vortex correlated with the rate of increase in hydraulic forces when the vortex reached the pump impeller. Fluctuation of hydraulic forces increased in proportion to the diameter. The maximum value of fluctuation with submerged vortex cavitation was approximately 1.4 times higher than that measured without vortex cavitation.

## Acknowledgments

We would like to thank Dr. T. Shibata and Mr. R. Iwano of Power & Industrial Systems R & D Lab., Hitachi, Ltd. for their valuable advice. We also wish to express thanks to Mr. T. Sato of Power & Industrial Systems Industrial Machinery Systems Division, Tsuchiura Products Division, Hitachi, Ltd. for his support of CFD computation.

## References

Arndt, R.E.A. and Keller, A.P. (1992). ASME J. Fluid Engineering, 114, 430-438.
Krishnamoorthy, S. and Marshall, J.S. (1998). Physics of Fluids, 10, No. 3, 2828-2845.
Rajendran, V.P., Constantinescu, G.S. and Patel, V.C. (1998). ASME Proceedings of FEDSM98-5098.
Shibata, T., Iwano, R., Nagahara, T. and Okamura, T. (2000). IAHR. Symposium Proceedings, 2B-CFD-G03.